Journal of Interfaces, Thin films, and Low dimensional systems 2 (2) Winter and Spring (2019) 183-194

Effects of hydrostatic pressure and temperature on the AlGaN/GaN high electron mobility transistors

Rajab Yahyazadeh* and Zahra Hashempour

Department of Physics, Khoy branch, Islamic Azad University, Khoy, Iran

ARTICLE INFO

Article history:
Received 21 May 2019
Revised 4 December 2019
Accepted 14 January 2020
Available online 1 February 2020

Keywords:
Temperature
Pressure
Effective mass
AlGaN/GaN HEMTs
Cut-off frequency

ABSTRACT

In this paper, the drain-source current, transconductance, and cutoff frequency in AlGaN/GaN high electron mobility transistors have been investigated. In order to obtain the exact parameters of AlGaN/GaN high electron mobility transistors such as the electron density, wave function, band gap, polarization charge, effective mass, and dielectric constant, the hydrostatic pressure and temperature effects are taken into account. It has been found that the drain-source current decreases as the temperature increases and increases as the hydrostatic pressure increases. The increase in temperature is equivalent to a negative virtual gate while an increase in the hydrostatic pressure is equivalent to the positive virtual gate voltage. Moreover, the temperature, hydrostatic pressure, and effective mass dependence in high electron mobility transistor structures are investigated. It is observed that the increase of hydrostatic pressure decreases the effective mass as the wave function penetrates through the quantum barrier AlGaN. In general, the process of increasing and decreasing the cutoff frequency and transconductance is similar to the variations in the drain-source current. The calculated results are in good agreement with the existing experimental data.

1 Introduction

AlGaN/GaN heterostructure field-effect transistors (HFETs) are of interest in RF applications because of their outstanding high-frequency and high-power performance [1–3]. Linearity is one of the most crucial figures of merit for the application of power amplifiers. For improving the device linearity, advanced device structures or epitaxial structure engineering, such as field plate, nonlinear polarization dielectric, double-channel, and optimized barrier or cap layer thickness, have been explored [4–7]. The two-dimension electron gas (2DEG) in AlGaN/GaN interface is the major carrier for the high efficient electronic transport which was commonly assumed to be related to the piezoelectric polarization of the strained AlGaN layer together with the spontaneous polarization. Understanding and controlling the transport behavior of carriers across the heterojunction interface is important for the optimization of their performance. Many reports have detailed the enhanced performance of piezotronic devices tuned by external mechanical strain/stress, including piezotronic enhanced photodetectors [8]. With the coupling of piezoelectric polarization with semiconductor properties in III-nitride materials, it is suggested that

*Corresponding author.
Email address: Yahyazadehs@Gmail.com
DOI: 10.22051/jitl.2020.26104.1031

III-nitride high electron mobility transistors (HEMTs) may be excellent candidates as strain-tunable transistors, since they have potential applications in electromechanical sensing, actuating, and mechanical energy harvesting. The current collapse through structural design and relieving the self-heating of the device are two effective efforts to tune/control the performance of AlGaN/GaN HEMTs [9]. More recently, the drain-source current of III nitride-based HEMT has been modeled by several groups [10-12]. It is important to investigate systematically the dependence of AlGaN–GaN HEMT performance on the hydrostatic pressure and temperature by including different physical parameters. In the present work, a new numerical model for the drain-source current of AlGaN/GaN HEMTs is presented. That is capable of determining the effects of hydrostatic pressure and temperature on the effective mass, barrier thickness, band gap, drain-source current, transconductanc, and cutoff frequency. One of the important advantages of this numerical method and the aspect of innovation in this work is the use of five important parameters; effective mass, band gaps, lattice constants, dielectric constant, and barrier thickness that are simultaneously dependent on pressure and temperature. In addition, the effect of self-heating, multisub-band, and polarization coulomb field scatterings on the mobility and electron density of quantum wells is used in the self-consistent solution of the Schrödinger equation. It should be noted that in this work the atmospheric pressure is associated with hydrostatic pressure ($P = P_{hydro} + P_{atm}$). That is, at zero hydrostatic pressure is the only atmospheric pressure applied while the fringing-field effect can be ignored.

2 Modelling HEMT

2.1 Self consistent solution of the Schrödinger-Poisson equations

In order to obtain accurate values for the Fermi energy, the energies of quantized levels within the 2DEG, potential profiles, wave function, and the sheet carrier concentration for the 2DEG in AlGaN/GaN heterostructures, both for the Schrödinger and Poisson equations must be solved self-consistently. This has been achieved by solving Schrödinger's equation and simultaneously taking into account the electrostatic potential obtained from Poisson's equation, as well as the image and exchange-correlation potentials using the three-point finite difference method. The Schrodinger equation is introduced to solve the wave function of electrons in the quantum structures:

$$-\frac{\hbar^2}{2m_e^*}\nabla^2\psi_n + V\psi_n = E_n\psi_n, \qquad (1)$$

where $\hbar$ represents the reduced Planck constant, m_e^* represents the electron e□ective mass, V represents the potential function, and ψ_n represents the nth state wave function, with its associated nth state energy level E_n. The electron effective mass m^* can be written as [14]

$$\frac{m_0}{m_e^*(P,T,m)} = 1 + \frac{E_P^{\Gamma}\left(E_g^{\Gamma}(P,T,m) + 2\Delta_{SO}/3\right)}{E_g^{\Gamma}\left(E_g^{\Gamma}(P,T,m) + \Delta_{SO}\right)}, \qquad (2)$$

where m_0 is the free electron mass, E_P^{Γ} is the energy linked to the momentum matrix element, Δ_{SO} is the spin-orbit splitting, and $E_g^{\Gamma}(P,T,m)$ is the band gap variation as a function of the hydrostatic pressure and temperature. E_g^{AlGaN} is given by [15-17]

$$E_g^{AlGaN}(T,P) = xE_g^{AlN}(T,P) + (1-x)E_g^{GaN}(T,P) - x(1-x), \qquad (3)$$

where E_g^{AlGaN} is the band gap from $E_g^{AlN}(T,P)$ and $E_g^{GaN}(T,P)$ respectively, as [16]

$$E_g(T,P) = E_g(0,0) + \gamma P + \sigma P^2 + \frac{\alpha T^2}{T+T_e} \qquad (4)$$

$E_g(0,0)$, stands for the band gap energy of GaN or AlGaN in the absence of the hydrostatic pressure at a temperature of zero Kelvin. The suggested parameters used in Eq. (4) of the present study have been taken from Ref [14].

The Poisson equation relates the electrostatic potential with spatial charge distribution written as

$$\kappa\nabla^2\varphi = -\rho + \nabla P_{tot}, \quad (5)$$

where φ is the potential distribution and ρ is the net charge which is a nonlinear function of the potential:

$$\rho(\varphi) = [p(\varphi) + n(\varphi) + N_D^+ - N_A^-], \quad (6)$$

where p and n denote the mobile carrier density of the holes and electrons, N_D^+ and N_A^- are the totally ionized donor and acceptor densities. $P_{tot} = P_{SP} + P_{PZ}$, denotes the total polarization vector that is composed of spontaneous polarization P_{SP} and strain-induced piezoelectric polarization P_{PZ}. By using the Al mol fraction (m), the lattice constant (a) and the strain (ϵ) can be obtained from [18, 19]

$$P_{GaN}^{PZ} = -0.918\epsilon + 9.541\epsilon^2, \quad (7)$$

$$P_{AlN}^{Pz} = \begin{cases} -1.808\epsilon + 5.624\epsilon^2 & for\ \epsilon < 0 \\ -1.808\epsilon - 7.888\epsilon^2 & for\ \epsilon > 0 \end{cases}$$

$$P_{AlGaN}^{SP} = 0.090m - 0.034(1-m) + 0.21x(1-m).$$

The basal strain is expressed from the lattice of substrate a_s and the epilayer $a_e(T,P,m)$:

$$\epsilon(T,P,m) = \frac{a_c - a_e(T,P,m)}{a_e(T,P,m)}. \quad (8)$$

The lattice constant as a function of temperature, alloy, and the hydrostatic pressure is given by [20, 21]

$$a_e(T,P,m) = a_0(m) \times \left[\left(1 + \beta\left(T - T_{ref}\right)\right)\left(1 - \frac{P}{3B_0}\right)\right], \quad (9)$$

where $B_0 = 239GPa$ is the bulk modulus of sapphire, $\beta_{GaN} = 5.56 \times 10^{-6}K^{-1}$ is the thermal expansion coefficient, and $T_{ref} = 300K^0$. The equilibrium lattice constant is represented by $a_0(m)$, where as a function of composition is given by [22, 23]

$$a_0(m) = 0.13989m + 0.03862. \quad (10)$$

The piezoelectric polarization is defined by Vergard's law as

$$P_{AlGaN}^{Pz} = mP_{AlN}^{PZ} + (1-m)P_{GaN}^{PZ}. \quad (11)$$

The total polarization at the interface AlGaN/GaN is expressed as

$$\sigma_s(T,P,m) = \left|P_{Al_mGa_{1-m}N}^{PZ} + P_{Al_mGa_{1-m}N}^{SP} - P_{GaN}^{SP} - P_{GaN}^{PZ}\right|. \quad (12)$$

2.2 Electron concentration

To calculate the total conduction electron concentration, the sheet density of electrons in each sub-band is found. The total density of electrons ($n = n_{2D} + n_{3D}$), the two and three-dimensional density electrons (n_{2D} and n_{3D}), is given as [24]

$$n_{2D} = \sum_i n_i = \sum_i \frac{m^* k_B T}{\pi\hbar^2} \ln\left[1 + \exp\left\{\frac{\left(E_f - E_i\right)}{k_B T}\right\}\right]|\psi_i|^2, \quad (13)$$

$$n_{3D} = \frac{2}{\sqrt{\pi}N_C F_{1/2}((E_F - E_C)/k_B T)}. \quad (14)$$

Equation (13) includes the density of each sub-band and gives the total sheet density of electron. Equation (13) gives the three-dimensional electron density. Here, $F_{1/2}$ is the Fermi integral of order 1/2.

By knowing E_i, the $2DEG$ density and the Fermi energy can be calculated from [25, 26]

$$n_{2D}(T,m,x,P) = \frac{\varepsilon_0\varepsilon(m,T,P)}{(d_d(T,P) + d_i + \Delta d)} \times (V_{GS} - V_T - E_F - V_{CH}(x)), \quad (15)$$

$$V_T = V_{BI} - \Delta E_c(m,T,P) - \frac{\sigma_{Pz}(m,T,P)d_d}{\varepsilon_0\varepsilon(m,T,P)} - \frac{qN_D d_d^2}{\varepsilon_0\varepsilon(m,T,P)}, \quad (16)$$

$$\varepsilon^{GaN}(T,P) = 10.28 \times exp(10^{-4}(T-T_0) - 6.7 \times 10^{-3}P), \quad (17)$$

$$\varepsilon^{AlGaN}(m,T,P) = \varepsilon^{GaN}(T,P) + 0.03m, \quad (18)$$

where $\varepsilon^{GaN}(T,P)$ and $\varepsilon^{AlGaN}(m,T,P)$ are the dielectric constant [27,28]. d_{AlGaN}, is the AlGaN barrier thickness [15,28]

$$d_{Al_mGa_{1-m}N}(T,P) = d_{AlGaN}(0)\left[-\left(S_{11}^{Al_mGa_{1-m}N} + 2S_{12}^{Al_mGa_{1-m}N}\right)P\right], \quad (19)$$

where $d_{AlGaN}(0)$ is the AlGaN layer thickness without hydrostatic pressure and temperature variations. S_{11}, S_{12} are the elastic compliance constants of $Al_mGa_{1-m}N$ that are given by [14, 28]

$$S_{11} = \frac{C_{11}C_{33} - C_{13}^2}{(C_{11}-C_{12})[C_{33}(C_{11}+C_{12}) - 2C_{13}^2]},$$

$$S_{12} = \frac{C_{12}C_{33} - C_{13}^2}{(C_{11}-C_{12})[C_{33}(C_{11}+C_{12}) - 2C_{13}^2]}, \quad (20)$$

Note that $V_{CH}(x)$, is the channel potential while $\Delta d = 1/n_{2D}\int z n_{2D}(z)dz$ represents the effective width of the two dimensional quantum well [23]. ΔE_C is the conduction band offset between AlGaN and GaN; It should be mentioned that to calculate the conduction band discontinuity in the AlGaN/GaN interface, the temperature and hydrostatic pressure dependence of the energy band gap has been taken into account as [16]

$$\Delta E_C(T,P) = 0.75\left(E_g^{AlGaN}(T,P) - E_g^{GaN}(T,P)\right). \quad (21)$$

2.3 Electron concentration

In order to obtain accurate values for mobility, the nonlinear formalism of the polarization–induced field as a function of Al mole fraction in AlmGa1-mN/GaN HEMTs has been assumed; moreover, intersub-band coupling coefficients (H_{mn}) as well as all fully- and partially–occupied sub-bands within two dimensional quantum well are taken into account. From the definition of the drift mobility we obtain [29-31]

$$\mu_{2DEG}(T,E) = \frac{e}{m^*}\langle\tau_{total}(T,E)\rangle, \quad (22)$$

where τ_{total} is the total relaxation times associated with PCF scattering and other main scattering mechanisms. These relaxation times have been calculated using the methods described in Refs [25] and [29-32]. Moreover, the different scattering rates can be separated into two types: (i) elastic scattering due to acoustic and piezoelectric phonons, ionized impurities, and interface roughness, etc., and (ii) inelastic scattering due to polar optical phonons. In order to take into consideration all scattering mechanisms in the mobility calculation, it is necessary to include all such mechanisms in the linearized Boltzmann equation to solve it numerically using an iterative technique [33]. It should be noted that in the linearized Boltzmann equation, $\Phi(E,T)$ is the perturbation function. In order to obtain $\Phi(E,T)$, it is needed to take into account the contribution of all occupied sub-bands [34]:

$$\frac{1}{\Phi(E,T)} = \sum_m\sum_n \frac{n_m}{n_{2DEG}}\frac{1}{\Phi_{mn}}. \quad (23)$$

Equation (23) indicates that all occupied states contribute towards the total mobility of the two-dimensional electron gases. This equation also shows that the contribution of each sub-band depends on its occupation number such that the most significant contribution comes from the first sub-band, which has the highest occupation

number. Using such an approach, it is possible to calculate the 2D-electron mobility by taking into account the combined contributions from each of the individual electron scattering mechanisms

3 Drain-source current

The drain-source current is given by [11, 12], and [23]:

$$I_{DS} = \begin{cases} Wqv(T,m,E)n_{2D}(V_{GS},x,m.T.P) - qD(T,E) \\ \dfrac{dn_{2D}(V_{GS},x,m,T,P)}{dx} \quad Linear\ region, \\ Wqv_{sat}(T,m)n_{2D}(V_{GS},x,m,T,P) - qD(T) \\ \dfrac{dn_{2D}(V_{GS},x,m.T,P)}{dx} \quad saturation\ region, \end{cases} \tag{24}$$

where the first term is the drift current while the second term is the diffusion current, W is the gate width, E is the electric field, $v(T,m,E)$ is the electron drift velocity, and $D(T,m)$ is the electron diffusion constant which can be assumed to be related to the mobility via the classical Einstein relation for low fields given by $D(T,m) = k_B T\mu(T)/q$ However, in order to solve Eq. (24), it is necessary to invoke the following boundary condition at the source and drain ends of the channel region:

$$V_{ch}(0) = I_{DS} \times (R_S(V_{GS}) + R_C),$$

$$V_{ch}(L_{SG} + L_G + L_{GD}) = V_{DS} - I_{DS} \times (R_D(V_{GS}) + R_C). \tag{25}$$

The contact resistance (R_C) is a constant value during the parameter measurement, the value variation of R_S results from the gate-source channel resistance. As a result, R_S and R_D are determined by the polarization coulomb field and other scattering mechanisms for the electrons in the gate-source channel [35, 36]. L_{SG},L_G and L_{GD}, are the lengths of the ungated distance between the source and gate, the gate length, and the ungated distance between the gate and drain, respectively. As it is inferred from the equations, the transport parameters of the 2-DEG are dependent upon temperature; however, the device temperature is different from the electron gas channel temperature because of the SH effects. During the calculations, the SH effect has been considered as stated in the following. The temperature difference between the channel and the bottom of the substrate ($\Delta T = T_{ch} - T_{sub}$) is [37]

$$\frac{\Delta T}{T_{sub}} = \frac{(1 - (P_{diss}/4P_0)^4)}{(1 - P_{diss}/4P_0)^4}, \tag{26}$$

where $T_{ch}$is the channel temperature, T_{sub} is the temperature of the substrate bottom,, $P_{diss} = I_{DS}V_{DS}$ is the power dissipation, P_0 is referred to as a quality factor with power dimension

$$P_0 = \frac{\pi K_{GaN}(T_{sub})WT_{sub}}{ln(8\,t_{sub}/\pi L_G)}. \tag{27}$$

Here, t_{sub} is the thickness of the substrate, L_G is the gate length, and $K_{GaN}(T_{sub}) = 1.6\left(T_{Sub}/300\right)^{-1/4}$is the thermal conductivity.

4 Cut-off frequencies

Knowing the current-voltage characteristics, one can find small-signal parameters such as the extrinsic transconductance (g'_m), the drain conductance (g_d), and the gate-to-source capacitance(C_{GS}). The transconductance and drain conductance can be defined by differentiating I_{DS} with respect to V_{GS} and V_{DS}, where V_{DS} and V_{GS} are kept constant, respectively.

By knowing these parameters, one can calculate the cutoff frequency, f_T, which is calculated as [19]

$$f_T(T,P,m) = \frac{g'_m(T,P,m)}{2\pi\left(C_{GS}(T,P,m) + C_{GD}(T,P,m)\right)}, \tag{28}$$

$$g'_m(T,P,m) = \frac{g_m(T,P,m)}{1 + g_m R_s(V_{GS})}. \quad (29)$$

Three kinds of carrier concentration contribute towards the gate-to-source (drain) capacitance. These are the carrier concentrations for the two-dimensional electron gas, free carriers, and neutralized donors in the barrier layer. Therefore, the gate-to-source (drain) capacitance is given by [40, 41]

$$C_{GS}(C_{GD}) = \sum_{k=0}^{3} qWL_G \frac{\partial n_k}{\partial V_{GS}(V_{DS})}. \quad (30)$$

The subscripts 1, 2, and, 3 refer to the 2DEG, free electrons, and neutralized donors in the barrier layer, respectively.

5 Results and discussion

In this paper, we present a numerical model for calculating the drain-source current of the AlGaN/GaN field effect transistors, which simultaneously investigates the influence of the hydrostatic pressure and temperature. To obtain a self-consistent solution of basic equations, iteration between the Schrödinger–Poisson equation systems is conducted by a three-point finite di□erence method. During the self-consistent calculation, A grid spacing as small as $1 \times 10^{-10} m$ along the z-axis and the convergent criteria for the electrostatic potential is set to be 0.1% to ensure the iteration convergence and stability of our calculations. Flow chart of the flow calculation program is solvable in a self-consistent manner according to Figure 1. To assess the validity of the numerical model for the drain-source current a comparative study has been undertaken to compare theoretically obtained, I_{DS} and curves with experimental results. The experimental results, material and device details, and all other material parameters have been taken from Refs [13, 14], [16, 17] for $Al_{0.24}Ga_{0.76}N/GaN$ HEMTs. Figure 2 shows the dependence of the AlGaN band-gap energy on the temperature and hydrostatic pressure. To investigate the physical concept of these effects, we first investigate the quantum well current density in terms of the gate voltage at different pressures and temperatures. As shown in Figure 2, the electron density of the quantum well and the threshold voltage decreases (the minimum voltage required for the quantum well).

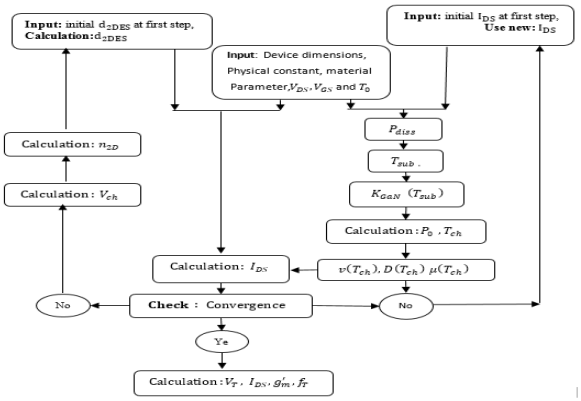

Figure 1. The 2D transport model analysis steps.

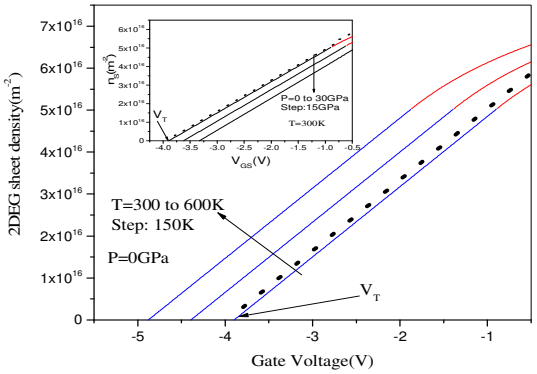

Figure 2. Variations of the 2DEG sheet density as a function of the Gate source voltage at different hydrostatic pressures. Insert: variations of the 2DEG sheet density as a function of the Gate source voltage at different temperature. The experimental data (symbols) and other needed parameters have been taken from Ref [42].

As the temperature increases to 300 K relative to the room temperature, the threshold voltage decreases by an absolute magnitude of 1V and an electron density of $1.65 \times 10^{16} m^{-2}$. The figure of the insert in Figure 2 indicates the electron density dependence on the hydrostatic pressure at different gate voltages. As the hydrostatic pleasure increases to 30 Gpa relative to the atmospheric pressure, the threshold voltage increases by an

absolute magnitude of 0.5 V and an electron density of $0.8 \times 10^{16} m^{-2}$. The threshold voltage depends on the total polarization charges (an important factor in the quantum well formation). Thus, as shown in Figure 3, AlGaN polarization (Piezoelectric and spontaneous) and bound charge at the hetrointerface (σ_b) increases when the hydrostatic pressure increases. With the increase in hydrostatic pressure, the lattice constants $(a_e(T,P,m), a_0(m))$ and occupancy of the various sub-bands (n_i) increase. This is due to the threshold voltage variations and the electron density of the quantum well. According to Figure 4 at 300K and hydrostatic pressure 0GPa (atmospheric pressure), the band-gap energy of AlGaN is 3.8 eV. The band-gap energy decreases with increasing temperature and increases with increasing hydrostatic pressure. The main cause of these changes is related to the quantum well depth changes. As the pressure increases, the band discontinuity and the threshold voltage (Eqs. (16) and (21)) increases. But as the temperature increases, these two parameters decrease. By comparing the band-gap energy variations with respect to temperature and pressure, it is observed that the hydrostatic pressure related changes are greater than temperature related changes. Figure 5 shows the dependence of the energy gap of GaN on the temperature and hydrostatic pressure.

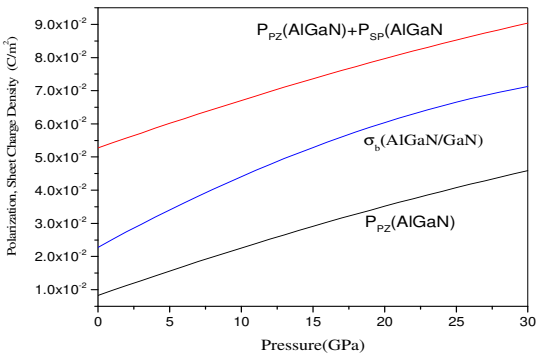

Figure 3. The variation of AlGaN polarization (Piezoelectric and spontaneous) and bound charge at the hetrointerface (σ_b) as a function of the hydrostatic pressure.

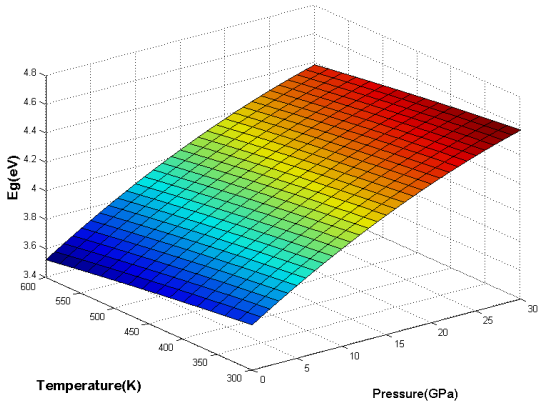

Figure 4. The band-gap energy of AlGaN as a function of hydrostatic pressure and temperature for $Al_{0.24}Ga_{0.76}N/GaN$ HEMTs.

The band-gap energy variations in this Figure are similar to the changes in Figure 4. Figure 6 shows the changes in the effective electron mass relative to the temperature and hydrostatic pressure. According to Figure 6, as the temperature increases, the effective electron mass increases and decreases with increasing hydrostatic pressure. As the effective electron mass decreases, the mobility of electrons in the quantum well increases. Therefore, an increase in the hydrostatic pressure is needed to increase the mobility of the electrons.

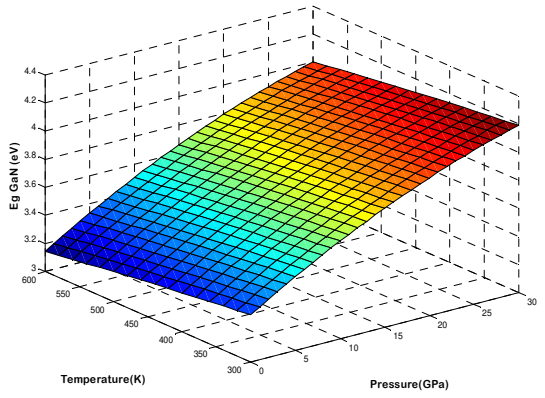

Figure 5. The band-gap energy of GaN as a function of hydrostatic pressure and temperature for $Al_{0.24}Ga_{0.76}N/GaN$ HEMTs.

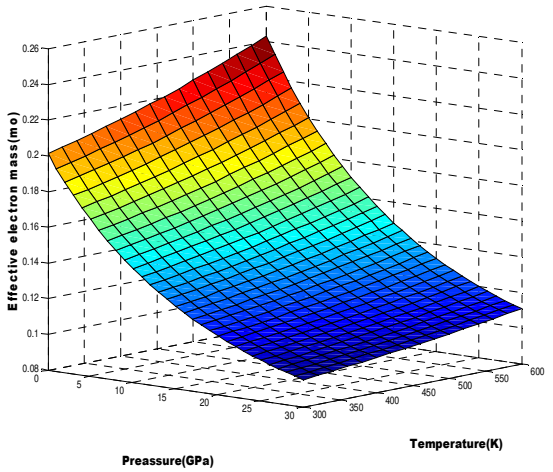

Figure 6. The effective electron mass of GaN as function of hydrostatic pressure and temperature for the $Al_{0.24}Ga_{0.76}N/GaN$ HEMTs.

Figure 7 shows the electron wave functions in the quantum well in terms of distance in different gate voltages. z=0 is the AlGaN/GaN interface. In Figure 7, with the increase of the gate voltage, the electron wave functions and electron density of the quantum well increases. The figure of the insert in Figure 7 indicates the electron wave function impenetrable to the AlGaN barrier. In Figure 8, the wave functions of the quantum well at different temperatures and a constant hydrostatic pressure are shown. In this figure, with increasing temperature, the height of wave functions and the corresponding electron density decrease. By comparing this figure with Figure 7, the temperature is as high as 600K; the electron density is decreased. As shown in the figure, the increase in temperature causes more electron wave functions to penetrate the quantum barrier, leading to an increase in the effective mass and a decrease in the mobility and density. As the temperature rises to 600K, the penetration of wave functions rises from 3500 to 4800. In Figure 9, the wave functions of the quantum well at different hydrostatic pressures and constant temperatures are shown. In this figure, with increasing the hydrostatic pressure, the height of wave functions and the corresponding electron densities increase. As the figure shows, the increase in hydrostatic pressure causes a decreases in the electron wave functions to penetrate the quantum barrier, leading to a decrease in the effective mass and an increase in mobility and density.

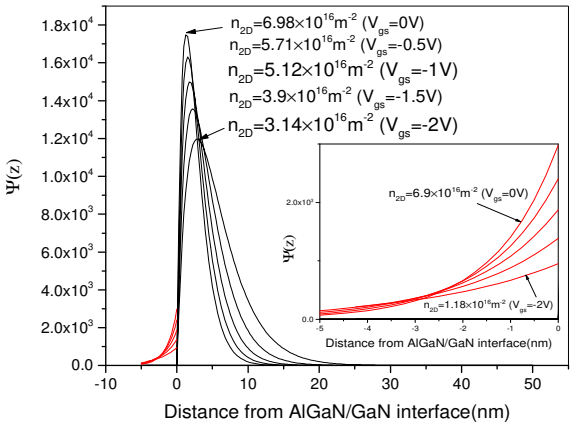

Figure 7. The electron wave function ψ(z) as a function of the distance from the AlGaN/GaN interface under different n_{2D} (here n_{2D} corresponds to the electron density under the gate region as a function of gate bias).

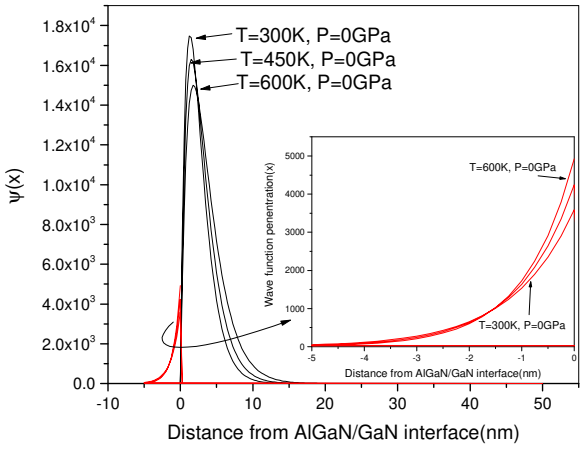

Figure 8. The electron wave function ψ(z) as a function of the distance from the AlGaN/GaN interface under different temperature without hydrostatic pressure. The insert indicates the electron wave function impenetrate to the AlGaN barrier.

The increase in hydrostatic pressure of 30GPa, reduces the penetration of wave functions from 3800 to 2800. Figure 10 shows the drain-source current variation in terms of the drain-source voltage AlGaN/GaN HEMTs at various temperatures and hydrostatic pressures. In the

saturation region, there is a negative conductivity which is a contribution to this decrease in the drain-source current due to the thermal effect partly due to the influence of wave functions on the quantum barrier AlGaN that increases the effective mass at high drain-source voltages. According to this figure, the temperature increase reduces the drain-source voltage. This decrease is higher in the saturation region than in the linear region, which is related to the reduction electron wave functions, the electron density of quantum well. This increases the effective mass and penetration of wave functions to the barrier.

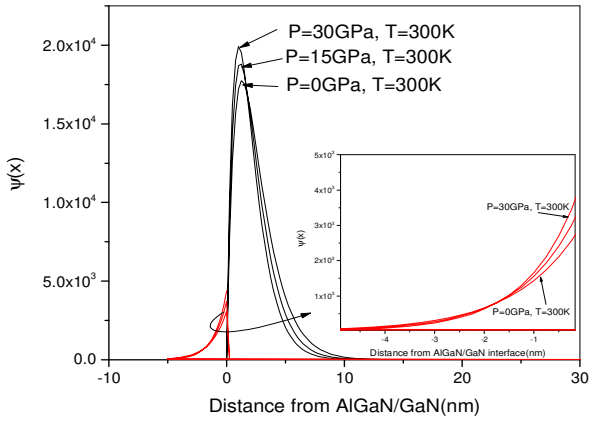

Figure 9. The electron wave function ψ(z) as a function of the distance from the AlGaN/GaN interface under different hydrostatic pressures and without temperature. The insert indicates the electron wave function impenetrate to the AlGaN barrier.

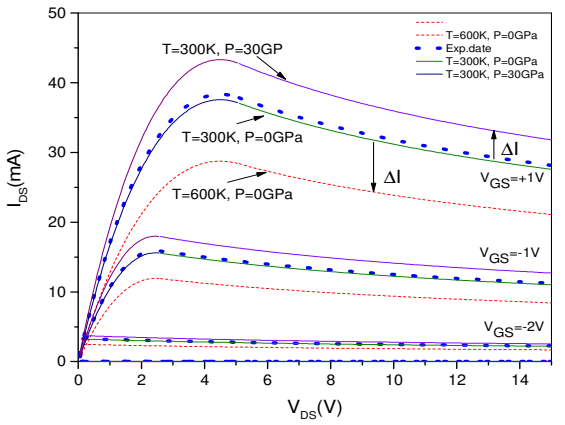

Figure 10. Drain current versus source–drain voltage for the $Al_{0.24}Ga_{0.76}N/GaN$ HEMTs, including temperature and temperature pressure effect in comparison with experimental data [13].

Increasing the hydrostatic pressure increases the piezoelectric polarization charge density and the drain-source current. Decreasing changes with increasing temperature relative to the incremental hydrostatic pressure changes are related to the effect of self-heating and the effect of penetration. According to Figure 11, the highest cutoff frequency is at 9.6 GHz and in the current range of 200 where the maximum g_m is located. As seen in Figure 11, when I_{DS} is greater than 200; the cutoff frequency continues with a lower reduction compared to transconductance. The further decrease in transconductance is related to the self-heating and penetration of the wave functions to the AlGaN barrier. In this figure, with increasing temperature, both the cut-off frequency and the transconductance are reduced, which is the reason for the decrease in the drain-source current. Figure 12 shows the cutoff frequency and mutual conductivity in terms of drain-source current at various pressures. As the pressure increases, the cutoff frequency and transconductance increases. This increase confirms the increase in drain-source current with the pressure at various voltages of Figure 9. In general, the process of increasing and decreasing the cutoff frequency and transconductance is similar to the variations in the drain-source current.

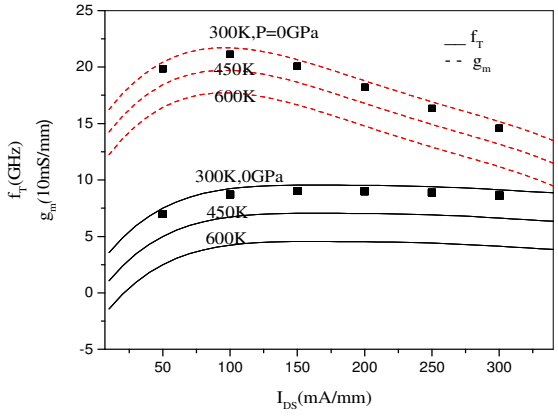

Figure 11. The cutoff frequency and transconductanc versus drain current in different temperature for $Al_{0.24}Ga_{0.76}N/GaN$ HEMTs. The experimental data and other needed parameters have been taken from Refs [38].

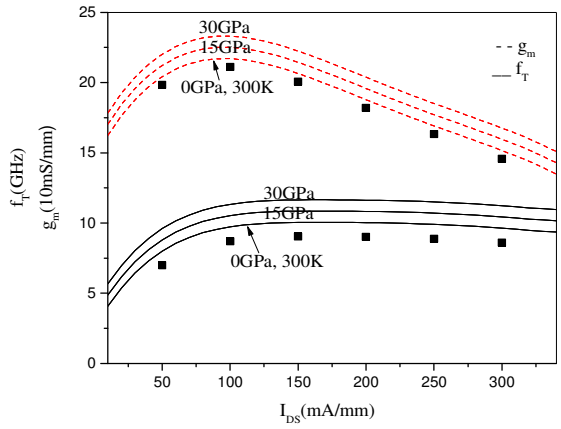

Figure 12. The cutoff frequency and transconductanc versus drain current at different hydrostatic pressure for the AlGaN/GaN HFET. The experimental data and other needed parameters have been taken from Refs [38].

5 Conclusions

In this paper, an accurate numerical model has been developed for the drain-source current of AlGaN/GaN-based HEMTs. This model is able to accurately predict the dependence of drain-source current, electron density and effective electron mass on the temperature and hydrostatic pressure. From the results, it is apparent that the temperature is as high as 300; the electron density is decreased to $1.65 \times 10^{16} m^{-2}$ and the penetration of wave functions rises from 3500 to 480. This increase in temperature is similar to the virtual gate of -1V. The increase in pressure of 30GPa reduces the penetration of wave functions from 3800 to 2800 and the electron density is increased to $0.8 \times 10^{16} m^{-2}$. This increase in hydrostatic pressure is similar to the virtual gate of +0.5V. Decreasing the drain-source current with increasing temperature is related to the effect of self-heating and penetration to the quantum barrier, but increasing the drain-source current with increasing pressure is related to the piezoelectric polarization. This decrease is higher in the saturation region than in the linear region. In general, the process of increasing and decreasing the cutoff frequency and transconductance is similar to the variations in the drain-source current.

Acknowledgments

The authors would like to thank Khoy Branch (Islamic Azad University) for the financial support of this research, which is based on the research project contract.

References

[1] L. Rey, A. D. Latorre, F. F. M. Sabatti, J. D. Albrecht, and M. Sa. Lraniti, "Hot electron generation under large-signal radio frequency operation of GaN high-electron-mobility transistors." Applied Physics Letters, **111** (2017) 013506.

[2] J. Ma, E. Matioli, "Slanted tri-gates for high-voltage GaN power devices." IEEE Electron Device Letters, **38b** (2017) 1305.

[3] G. Tang, et al., "Digital integrated circuits on an E-mode GaN power HEMT platform." IEEE Electron Device Letters, **38** (2017) 1282.

[4] M. Blaho, et al., "Annealing temperature, and bias-induced threshold voltage instabilities in integrated E/D-mode InAlN/GaN MOS HEMTs." Applied Physics Letters, **111** (2017) 033506.

[5] K. Zhang, et al., "High-Linearity AlGaN/GaN FinFETs for Microwave Power Applications." IEEE Electron Device Letters, **38** (2017) 615.

[6] H. Chiu, et al., "RF Performance of in Situ SiNx Gate Dielectric AlGaN/GaN MISHEMT on 6-in Silicon-On-Insulator Substrate." IEEE Transactions on Electron Devices, **64** (2017) 4065.

[7] S. Sun, et al., "AlGaN/GaN metal-insulator-semiconductor high electron mobility transistors with reduced leakage current and enhanced breakdown voltage using aluminum ion implantation." Applied Physics Letters, **108** (2016) 013507.

[8] Z. Zhang, Q. Liao, Y. Yu, X. Wang, and Y. Zhang, "Enhanced photo response of ZnO Nano rods-based self-powered photo detector by

piezotronic interface engineering." Nano Energy, **9** (2014) 237.

[9] S. Yuan, B. Duan, X. Yuan, Z. Cao, H. Guo, and Y. Yang, "New Al0.25Ga0.75N/GaN high electron mobility transistor with partial etched AlGaN layer." Superlattices and Microstructures, **93** (2016) 303.

[10] Y. Chang, Y. Zhang, Y. Zhang, "Thermal model for static current characteristics of AlGaN/GaN high electron mobility transistors including self-heating effect." Journal of Applied Physics, **99** (2006) 044501.

[11] R. Yahyazadeh, A. Asgari, and M. Kalafi, "Effect of depletion layer on negative differential conductivity in AlGaN/GaN high electron mobility transistor." Physica E, **33** (2006) 77.

[12] Rashmi, A. Kranti, S. Haldar, M. G. Gupta, et al., "Comprehensive analysis of small-signal parameters of fully strained and partially relaxed high Al-content lattice mismatched AlmGa1-mN/GaN HEMTs." IEEE Trans on Microwave Theory Techniques, **52** (2003) 607.

[13] P. Cui, et al., "Influence of different gate biases and gate lengths on parasitic source access resistance in AlGaN/GaN heterostructure FETs." IEEE Transactions on Electron Devices, **64** (2017) 1038.

[14] I. Vurgaftman, J. R Meyer, L. R. R Mohan, "Band parameters for III–V compound semiconductors and their alloys." Journal of Applied Physics, **89** (2001) 5815.

[15] K. J. Bala, A. J Peter, and C. W Lee, "Simultaneous effects of pressure and temperature on the optical transition energies in a Ga0.7In0.3N/GaN quantum ring." Chemical Physics, **495** (2017) 42.

[16] N. E. Christensen, I. Gorczyca. "Optical and structural properties of III-V nitrides under pressure." Physical Review B, **50** (1994) 4397.

[17] Z. Dridi, B. Bouhafs, Ruterana. "Pressure dependence of energy band gaps for AlxGa1−xN, InxGa1−xN and InxAl1−xN." New Journal of Physics, **4** (2002) 94.1.

[18] O. Ambacher , A. B Foutz, J Smart, J. R. Shealy, N. G. Weimann, K. Chu et al., "Two dimensional electron gases induced by spontaneous and piezoelectric polarization in undoped and doped AlGaN/GaN heterostructures." Journal of Applied Physics, **87** (2000) 334.

[19] O. Ambacher, J. Majewski, C. Miskys, et al., "Pyroelectric properties of Al (In) GaN/GaN hetero- and quantum well structures." Journal of Physics: Condensed Matter, **14** (2002) 3399.

[20] Z. J. Feng, Z. J. Cheng, and H. Yue. "Temperature dependence of Hall electron density of GaN-based heterostructures." Chinese Physics, **13** (2004) 1334.

[21] V. Fiorentini, F. Bernardini, and O. Ambacher, "Evidence for nonlinear macroscopic polarization in III–V nitride alloy Heterostructures." Applied Physics Letters, **80** (2002) 1204.

[22] P. Perlin, L. Mattos, N. A. Shapiro, J. Kruger, W. S. Wong, T. Sands, N. W. Cheung, and E. R. Weber, "Reduction of the energy gap pressure coefficient of GaN due to the constraining presence of the sapphire substrate." Journal of Applied Physics, **85** (1999) 2385.

[23] K. Elibol, G. Atmaca, P. Tasli, and S. B. Lisesivdin, "A numerical study on subband of InxAl1-xN/InN-based HEMT structure with low-indum ($x < 0.01$) barrier layer." Solid state communication, **162** (2013) 8.

[24] R. Yahyazadeh, Analytical-numerical model for sheet resistance of $Al_xGa_{1-x}N/GaN$ high electron mobility transistors, Journal of Non - Oxide Glasses, **10** (2018) 57.

[25] P. Roblin, H. Rahdin, "High-speed Heterostructure Devices from Device Concepts to Circuit Modeling." Cambridge University Press, Cambridge (2002) 277.

[26] A. Agrawal, M .Gupta, R. S. Gupta, "RF performance assessment of AlGaN/GaN MISHFET at high temperatures for improved power and pinch-off characteristics." Microwave and Optical Technology Letters, **51** (2009) 1942.

[27] C. M. Duque, A. L. Morales, M. E. Mora-Ramos, and C. A. Duque, "Exciton-related optical properties in zinc-blende GaN/InGaN quantum wells under hydrostatic pressure." Physica Status Solidi (b), **252** (2015) 670.

[28] M. Yang et al., "Effect of polarization coulomb field scattering on parasitic source access resistance and extrinsic transconductance in AlGaN/GaN heterostructure FETs." IEEE Transactions Electron Devices, **63** (2016) 1471.

[29] L. Hsu, W. Walukiewicz, "Effect of polarization fields on transport properties in AlGaN/GaN heterostructures." Journal of Applied Physics, **89** (2001) 1783.

[30] H. Yu, K. F. Brennan, "Theoretical study of the two-dimensional electron mobility in strained III-nitride heterostructures." Journal of Applied Physics, **89** (2001) 3827.

[31] R. Yahyazadeh, "Effect of Temperature on the Total Mobility of AlGaN/GaN High Electron Mobility Transistors." ECS Transactions, **60** (2014) 1051.

[32] L. Yang et al., "Enhanced g_m and f_T with High Johnson's Figure-of-Merit in Tin Barrier AlGaN/GaN HEMTs by TiN-Based Source Contact Ledge." IEEE Electron Device Letters, **38** (2017) 1563.

[33] A. Asgari, M. Kalafi, and L. Faraone, "Effects of partially occupied sub-bands on two-dimensional electron mobility in AlxGa1−xN/GaN Heterostructures." Journal of Applied Physics, **95** (2004) 1185.

[34] T. Palacios, et al., "Influence of the dynamic access resistance in the gm and ft. linearity of AlGaN/GaN HEMTs." IEEE Transactions on Electron Devices, **52** (2005) 2117.

[35] M. Yang et al., "Effect of polarization coulomb field scattering on parasitic source access resistance and extrinsic transconductance in AlGaN/GaN heterostructure FETs." IEEE Transactions on Electron Devices, **63** (2016) 1471.

[36] Y. Chang, Y. Zhang, and Yu. Zhang. "A thermal model for static current characteristics of AlGaN/GaN high electron mobility transistors including self-heating effect." Journal of Applied Physics, **99** (2006) 044501.

[37] J. C. Freeman, Channel temperature model for microwave AlGaN/GaN power HEMTs on SiC and sapphire, IEEE MTT-S International Microwave Symposium Digest, **3** (2004) 2031.

[38] C. Anghel, A. M. Lonescu, N. Hefyene, R. Gillon, European Solid-State Device Research, 33rd Conference on. ESSDERC '03, (2003) 449.

[39] W. Jin, W. Liu, S. K. H. Fung, P. C. H. Chan, and C. Hu, "SOI thermal impedance extraction methodology and its significance for circuit simulation." IEEE Transactions on Electron Devices, **48** (2001) 730.

[40] T. H. Yu, K. F. Brennan, "Theoretical study of a GaN-AlGaN high electron mobility transistor including a nonlinear polarization model." IEEE Transactions on Electron Devices, **50** (2003) 315.

[41] Y. F. Wu, S. Keller, P. Kozodoy, B. P. Keller, P. Parikh, D. Kapolnek,S. P. Denbaars, and U. K. Mishra, "Bias Dependent Microwave Performance of AlGaN/GaN MODFET's Up To 100 V." IEEE Electron Device Letters, **18** (1997) 290.

[42] S. Turuvekere, et al., "Gate leakage mechanisms in AlGaN/GaN and AlInN/GaN HEMTs: Comparison an modeling" IEEE Transactions on Electron Devices, **60** (2013) 3157.